AUTHOR'S PERSONAL COPY

NASA TECHNICAL NOTE

NASA TN D-1949

NASA TN D-1949

FLUTTER OF FLAT RECTANGULAR ORTHOTROPIC PANELS WITH BIAXIAL LOADING AND ARBITRARY FLOW DIRECTION

by Herman L. Bohon;
Langley Research Center,
Langley Station, Hampton, Va.

NATIONAL AERONAUTICS AND SPACE ADMINISTRATION • WASHINGTON, D.C. • SEPTEMBER 1963

NATIONAL AERONAUTICS AND SPACE ADMINISTRATION

TECHNICAL NOTE D-1949

FLUTTER OF FLAT RECTANGULAR ORTHOTROPIC PANELS WITH BIAXIAL LOADING AND ARBITRARY FLOW DIRECTION*

By Herman L. Bohon

SUMMARY

A theoretical analysis is presented on the flutter of flat simply supported orthotropic panels at supersonic speeds. Modified piston theory is employed for the lateral loading. Flutter boundaries obtained by the Galerkin procedure are presented for square panels of various stiffness ratios with arbitrary orientation of maximum panel flexural stiffness with the airstream and various conditions of biaxial compressive loading.

The boundaries show that orthotropic panels are highly sensitive to small changes in flow angularity away from the condition of orientation of maximum stiffness in the direction of the stream. Further, a small change from this orientation can cause a change in the critical flutter mode, and there can be stress ratios for which very large thicknesses are required for prevention of flutter once the panel undergoes the mode change. The results also indicate that a choice of proper panel orientation should be based on an analysis which includes representative conditions on flow angularity and midplane loading. In addition, a method for determining the intersection of the linear dynamic and static stability boundaries is presented.

INTRODUCTION

The prevention of flutter of exposed skin surfaces of supersonic and reentry-type vehicles has become a critical design problem, as is evident from flutter experienced by recent vehicles operating at supersonic speeds. (See ref. 1.) Although numerous theoretical studies have been conducted (see ref. 2), the large number of parameters influencing a flutter boundary discourage comprehensive analytical studies. Furthermore, the experimentalists have extreme difficulty in isolating the various parameters in experimental investigations and, consequently, correlation between experimental and theoretical results is generally unsatisfactory.

---

*The information presented herein was offered as a thesis in partial fulfillment of the requirements for the degree of Master of Science in Engineering Mechanics, Virginia Polytechnic Institute, Blacksburg, Virginia, March 1963.

Some of the parameters known to have a large influence on the flutter boundary are panel geometry, edge restraints, and midplane compressive loads. In addition, recent theoretical studies (see refs. 3 and 4) indicated large effects of flow angularity (in the plane of the panel) on flutter of rectangular panels, free of midplane loads (ref. 3), and with midplane compression and shear (ref. 4). The theoretical analyses, however, have considered only flat or slightly curved isotropic panels and, with the exception of some treatment in reference 5, no theoretical investigations have been conducted on flutter characteristics of orthotropic panels.

The use of orthotropic panels (generally corrugation-stiffened panels) is widespread in design of exposed-skin construction of supersonic and reentry-type vehicles. In general, such panels have greater load-carrying ability per unit weight than the conventional isotropic panel and thus provide a weight saving. In addition, the corrugation-stiffened panel is adaptable to the severe temperature environment encountered at high supersonic speeds where alleviation of some thermal stresses is essential.

Theoretical and experimental data depicting the flutter behavior of orthotropic panels are practically nonexistent and the flutter characteristics of such panels must, of necessity, be determined by wind-tunnel investigations. (These investigations are sometimes rather extensive.) Thus, it is essential to evaluate the influence of parameters affecting the flutter characteristics of orthotropic panels.

The investigation reported herein will show the effects of flow angularity and biaxial compression on the flutter behavior of unbuckled orthotropic panels. A four-mode Galerkin-type approximation to the solution of the governing equation for lateral deflections is performed for simply supported rectangular orthotropic panels and linearized aerodynamics from modified piston theory is employed for the lateral loading. The problem of proper orientation of the panel with the airstream will be discussed.

SYMBOLS

$\overline{A},\overline{B}$ parameters defined by equations (10)

$\overline{A}_n$ stress parameter, $\dfrac{N_x a^2}{\pi^2 D_x} - 2n^2\left(\dfrac{a}{b}\right)^2 \dfrac{D_{xy}}{D_x}$

a panel length in x-direction

$\overline{B}_I,\overline{B}_R$ parameters defined by equations (18)

$\overline{B}_n$ frequency parameter, $n^2\left(\dfrac{a}{b}\right)^2\left[\dfrac{N_y a^2}{\pi^2 D_x} - n^2\left(\dfrac{a}{b}\right)^2 \dfrac{D_y}{D_x}\right] - g_a \dfrac{\alpha}{\omega_r} - \dfrac{\alpha^2}{\omega_r^2}$

$\bar{B}_R'$ parameter defined by equation (15b)

b panel width in y-direction

b_1, b_2, b_3, b_4 coefficients defined by equations (9)

$\bar{b}_1, \bar{b}_2, \bar{b}_3, \bar{b}_4$ coefficients defined by equations (19c)

C_{mn} Fourier series coefficients

c speed of sound

D_x maximum flexural stiffness of panel

D_y minimum flexural stiffness of panel

D_{xy} twisting stiffness of panel

d, e, k, p coefficients defined by equations (19b)

g_a aerodynamic damping coefficient, $\frac{\rho c}{\gamma \omega_r}$

Im imaginary part

$i = \sqrt{-1}$

j, l, m, n, r, s integers

K_x, K_y dimensionless measures of inplane buckling load in x- and y-directions, respectively

$\bar{L}_{mn,rs}$ generalized force coefficient defined by equations (6)

M Mach number

N_x inplane loading in x-direction, positive in compression

N_y inplane loading in y-direction, positive in compression

$N_{x,cr}, N_{y,cr}$ critical inplane loads

$\bar{P}_{mn,rs}$ generalized force coefficient defined by equations (6)

Q, R, S, R_o, S_o coefficients defined by equations (13) and (19b)

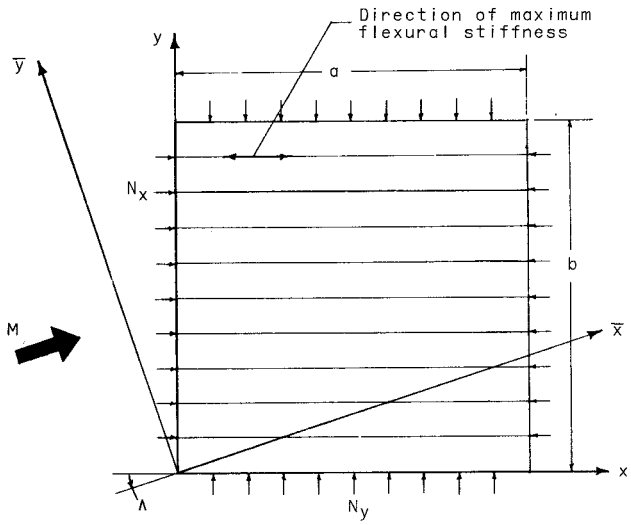

Figure 1.- Panel geometry and coordinate system.

q	dynamic pressure of air-stream, $\frac{\rho v^2}{2}$
Re	real part
t	time
v	flow velocity
w	lateral deflection of panel
x,y	Cartesian coordinates of panel (see fig. 1)
$\bar{x},\bar{y}$	fixed coordinates based on stream direction (see fig. 1)
α	frequency exponential coefficient
$\beta = \sqrt{M^2 - 1}$	
γ	mass per unit area of panel
η	nondimensional coordinate, y/b
Λ	flow angle in plane of panel, deg
λ	dynamic-pressure parameter, $\frac{2qa^3}{\beta D_x}$
λ_{cr}	critical value of dynamic-pressure parameter
λ_T	transtability speed
ξ	nondimensional coordinate, x/a
ρ	density of air
ψ	real part of complex frequency exponential coefficient
ω	circular frequency
ω_r	reference frequency (see eqs. (7))

Subscripts:

j,l,m,n,r,s	integers

ANALYSIS

An analysis of the governing equation for flutter of orthotropic rectangular panels with one surface exposed to supersonic flow is presented. The panel geometry and coordinate system are shown in figure 1. The panel has a length a in the x-direction (direction of maximum stiffness) and width b in the y-direction (direction of minimum stiffness). The flow direction in the plane of the panel is at an arbitrary angle Λ measured with respect to the direction of maximum panel stiffness. The effects of constant inplane loads are included and small deflections are assumed.

For small-deflection thin-plate theory the governing equation for vibrations of orthotropic panels subjected to supersonic flow over one surface is

$$D_x \frac{\partial^4 w}{\partial x^4} + 2D_{xy} \frac{\partial^4 w}{\partial x^2 \partial y^2} + D_y \frac{\partial^4 w}{\partial y^4} + N_x \frac{\partial^2 w}{\partial x^2} + N_y \frac{\partial^2 w}{\partial y^2} = -\gamma \frac{\partial^2 w}{\partial t^2} - \rho c \frac{\partial w}{\partial t} - \frac{2q}{\beta} \frac{\partial w}{\partial \bar{x}} \tag{1}$$

where D_x and D_y are the flexural stiffnesses in the x- and y-directions, respectively; D_{xy} is the twisting stiffness; N_x and N_y are constant inplane loads, positive in compression; and γ is the mass per unit area of the panel. The last two terms on the right-hand side of equation (1) represent the linearized lateral air forces given by modified piston theory. That is, the Mach number M in the last term on the right-hand side of equation (1) is replaced by β, where $\beta = \sqrt{M^2 - 1}$. In these terms, ρ is the density of air, c is the speed of sound, and q is the dynamic pressure.

After transformation of the loading term to the panel coordinates and nondimensionalization, equation (1) becomes:

$$\frac{\partial^4 w}{\partial \xi^4} + 2\left(\frac{a}{b}\right)^2 \frac{D_{xy}}{D_x} \frac{\partial^4 w}{\partial \xi^2 \partial \eta^2} + \left(\frac{a}{b}\right)^4 \frac{D_y}{D_x} \frac{\partial^4 w}{\partial \eta^4} + \frac{N_x a^2}{D_x} \frac{\partial^2 w}{\partial \xi^2} + \frac{N_y a^4}{D_x b^2} \frac{\partial^2 w}{\partial \eta^2}$$

$$+ \frac{\gamma a^4}{D_x} \frac{\partial^2 w}{\partial t^2} + \frac{\rho c a^4}{D_x} \frac{\partial w}{\partial t} + \frac{2qa^3}{\beta D_x} \left[(\cos \Lambda)\frac{\partial w}{\partial \xi} + \frac{a}{b}(\sin \Lambda)\frac{\partial w}{\partial \eta}\right] = 0 \tag{2}$$

where $\xi = \frac{x}{a}$ and $\eta = \frac{y}{b}$. The boundary conditions for a simply supported panel are:

$$\left.\begin{aligned} &w(0,\eta,t) = w(1,\eta,t) = w(\xi,0,t) = w(\xi,1,t) = 0 \\ &\frac{\partial^2 w}{\partial \xi^2}(0,\eta,t) = \frac{\partial^2 w}{\partial \xi^2}(1,\eta,t) = \frac{\partial^2 w}{\partial \eta^2}(\xi,0,t) = \frac{\partial^2 w}{\partial \eta^2}(\xi,1,t) = 0 \end{aligned}\right\} \tag{3}$$

A solution to equation (2) for these boundary conditions will be obtained by the Galerkin procedure as follows. Let the lateral deflection of the panel be represented by:

$$w = \mathrm{Re} \sum_m \sum_n \left(C_{mn} \sin m\pi\xi \sin n\pi\eta\right) e^{\alpha t} \tag{4}$$

where α, in general, is complex. This equation satisfies the boundary conditions term by term and the coefficients C_{mn} are arbitrary. Substituting equation (4) into equation (2), multiplying by $\sin r\pi\xi \sin s\pi\eta$, and integrating over the panel yields the following set of equations for the coefficients C_{mn}:

$$\left(m^4 - m^2\overline{A}_n - \overline{B}_n\right)C_{mn} + \frac{1}{\pi^4} \sum_{r=1}^{j} \sum_{s=1}^{l} \lambda(\cos \Lambda)\overline{L}_{mn,rs}C_{rn}$$

$$+ \frac{1}{\pi^4} \sum_{r=1}^{j} \sum_{s=1}^{l} \lambda \frac{a}{b}(\sin \Lambda)\overline{P}_{mn,rs}C_{ms} = 0 \qquad \begin{pmatrix} m = 1, 2, \ldots j; \\ n = 1, 2, \ldots l \end{pmatrix} \tag{5}$$

where

$$\left.\begin{aligned} \overline{L}_{mn,rs} &= 0 && n \neq s \\ &= 0 && m + r \text{ even}, \quad n = s \\ &= \frac{4mr}{r^2 - m^2} && m + r \text{ odd}, \quad n = s \\ \overline{P}_{mn,rs} &= 0 && m \neq r \\ &= 0 && n + s \text{ even}, \quad m = r \\ &= \frac{4ns}{s^2 - n^2} && n + s \text{ odd}, \quad m = r \end{aligned}\right\} \tag{6}$$

and

$$
\left.
\begin{aligned}
\lambda &= \frac{2qa^3}{\beta D_x} \\
\bar{A}_n &= \frac{N_x a^2}{\pi^2 D_x} - 2n^2\left(\frac{a}{b}\right)^2 \frac{D_{xy}}{D_x} \\
\bar{B}_n &= n^2\left(\frac{a}{b}\right)^2\left[\frac{N_y a^2}{\pi^2 D_x} - n^2\left(\frac{a}{b}\right)^2 \frac{D_y}{D_x}\right] - g_a \frac{\alpha}{\omega_r} - \frac{\alpha^2}{\omega_r{}^2} \\
\omega_r{}^2 &= \frac{\pi^4 D_x}{\gamma a^4} \\
g_a &= \frac{\rho c}{\gamma \omega_r}
\end{aligned}
\right\} \tag{7}
$$

In equations (7) ω_r is the lowest in vacuo frequency of a simply supported semi-infinite plate and g_a is the aerodynamic damping coefficient. A four-mode solution to equation (5) has been obtained with the use of two terms of the sine series of equation (4) in both the x- and y-directions ($m = 1,2$; $n = 1,2$). For a nontrivial solution, the determinant of the coefficients of C_{mn} must equal zero; thus, for $j = l = 2$,

$$
\begin{vmatrix}
b_1 & \frac{8}{3}\frac{\lambda}{\pi^4}\cos\Lambda & \frac{8}{3}\frac{a}{b}\frac{\lambda}{\pi^4}\sin\Lambda & 0 \\
-\frac{8}{3}\frac{\lambda}{\pi^4}\cos\Lambda & b_2 & 0 & \frac{8}{3}\frac{a}{b}\frac{\lambda}{\pi^4}\sin\Lambda \\
-\frac{8}{3}\frac{a}{b}\frac{\lambda}{\pi^4}\sin\Lambda & 0 & b_3 & \frac{8}{3}\frac{\lambda}{\pi^4}\cos\Lambda \\
0 & -\frac{8}{3}\frac{a}{b}\frac{\lambda}{\pi^4}\sin\Lambda & -\frac{8}{3}\frac{\lambda}{\pi^4}\cos\Lambda & b_4
\end{vmatrix} = 0 \tag{8}
$$

where

$$
\left.
\begin{aligned}
b_1 &= 1 - \bar{A} - \bar{B} \\
b_2 &= 16 - 4\bar{A} - \bar{B} \\
b_3 &= 1 - \bar{A} - \bar{B} + 6\left(\frac{a}{b}\right)^2 \frac{D_{xy}}{D_x} - 3\left(\frac{a}{b}\right)^2\left[K_y \frac{N_y}{N_{y,cr}} - 5\left(\frac{a}{b}\right)^2 \frac{D_y}{D_x}\right] \\
b_4 &= 16 - 4\bar{A} - \bar{B} + 24\left(\frac{a}{b}\right)^2 \frac{D_{xy}}{D_x} - 3\left(\frac{a}{b}\right)^2\left[K_y \frac{N_y}{N_{y,cr}} - 5\left(\frac{a}{b}\right)^2 \frac{D_y}{D_x}\right]
\end{aligned}
\right\} \tag{9}
$$

and

$$\left.\begin{aligned}\bar{A} &= K_x \frac{N_x}{N_{x,cr}} - 2\left(\frac{a}{b}\right)^2 \frac{D_{xy}}{D_x} \\ \bar{B} &= \left(\frac{a}{b}\right)^2\left[K_y \frac{N_y}{N_{y,cr}} - \left(\frac{a}{b}\right)^2 \frac{D_y}{D_x}\right] - g_a \frac{\alpha}{\omega_r} - \frac{\alpha^2}{\omega_r^2}\end{aligned}\right\} \tag{10}$$

In equations (9) and (10), K_x and K_y are dimensionless measures of the inplane buckling loads $N_{x,cr}$ and $N_{y,cr}$, respectively, defined by the following expressions:

$$\left.\begin{aligned}K_x &= \frac{N_{x,cr}a^2}{\pi^2 D_x} \\ K_y &= \frac{N_{y,cr}a^2}{\pi^2 D_x}\end{aligned}\right\} \tag{11}$$

Expansion of the determinant (eq. (8)) results in the following equation in λ:

$$Q\left(\frac{\lambda}{\pi^4}\right)^4 + R\left(\frac{\lambda}{\pi^4}\right)^2 + S = 0 \tag{12}$$

where

$$\left.\begin{aligned}Q &= \left(\frac{8}{3}\right)^4\left[\cos^2\Lambda - \left(\frac{a}{b}\right)^2\sin^2\Lambda\right]^2 \\ R &= \left(b_1b_2 + b_3b_4\right)\left(\frac{8}{3}\cos\Lambda\right)^2 + \left(b_1b_3 + b_2b_4\right)\left(\frac{8}{3}\frac{a}{b}\sin\Lambda\right)^2 \\ S &= b_1b_2b_3b_4\end{aligned}\right\} \tag{13}$$

No attempt has been made to reduce the expressions of equations (13) and the notation was adopted purely for convenience. It should be noted that for a specified panel, a/b, D_x, D_y, and D_{xy} are constants, and, by equations (10), $\bar{A}$ is seen to be a measure of the inplane load in the x-direction. Further, $\bar{B}$ is a function of the frequency coefficient α and the inplane load in the y-direction.

In the absence of damping, equation (12) can be solved by assuming simple harmonic motion; that is, let $\alpha = i\omega$, where ω is the circular frequency. Then the critical value of λ for flutter occurs when two roots ω of the frequency parameter $\bar{B}$ become equal or coalesce. (See refs. 6 and 7.) For values of λ

to and including λ_{cr}, all roots ω of the frequency parameter are real. For $\lambda > \lambda_{cr}$, the pair of roots of ω that coalesce become complex conjugates and, thus, the panel has at least one unstable mode of oscillation.

A method for the solution of equation (12) when aerodynamic damping is included is presented in references 6 and 8. This method will be outlined in the following discussion for the purpose of determining the flutter criterion and to develop equations from which numerical results for orthotropic panels at flow angle Λ will be obtained.

Let the frequency coefficient α and, consequently, the frequency parameter $\overline{B}$ be complex; that is, let

$$\left.\begin{aligned} \alpha &= \psi + i\omega \\ \overline{B} &= \overline{B}_R + i\overline{B}_I \end{aligned}\right\} \tag{14}$$

where ω is the circular frequency. Then, solving for α from the last of equations (10) yields

$$\alpha = \psi + i\omega = -\frac{g_a\omega_r}{2} \pm \sqrt{\left(\frac{g_a\omega_r}{2}\right)^2 - \omega_r^2\left(\overline{B}_R' + i\overline{B}_I\right)} \tag{15a}$$

where

$$\overline{B}_R' = \overline{B}_R - \left(\frac{a}{b}\right)^2\left[K_y \frac{N_y}{N_{y,cr}} - \left(\frac{a}{b}\right)^2 \frac{D_y}{D_x}\right] \tag{15b}$$

Equation (15a) may be examined to see what condition on g_a is required to make ψ vanish. For specified values of g_a the panel motion is stable if ψ is negative and unstable if ψ is positive. (See eq. (4).) Therefore, for flutter ($\psi > 0$) equation (15a) gives the following condition on g_a (refs. (6) and (8)):

$$\frac{\overline{B}_I^{\,2}}{\overline{B}_R'} > g_a^{\,2} \tag{16}$$

When the conditions for the panel on the threshold of instability ($\psi = 0$) are considered, equation (16) requires that

$$\overline{B}_I^{\,2} = g_a^{\,2}\overline{B}_R' \tag{17}$$

Substituting $\alpha = i\omega$ into the last of equations (10) gives the following expressions for $\overline{B}_R$ and $\overline{B}_I$:

$$\left.\begin{aligned}
\bar{B}_R &= \left(\frac{a}{b}\right)^2\left[K_y \frac{N_y}{N_{y,cr}} - \left(\frac{a}{b}\right)^2 \frac{D_y}{D_x}\right] + \left(\frac{\omega}{\omega_r}\right)^2 \\
\bar{B}_I &= -g_a \frac{\omega}{\omega_r}
\end{aligned}\right\} \tag{18}$$

Equations (14) and the condition on g_a (eq. (17)) permit rapid and direct solution of equation (12). Substituting the last of equations (14) into equation (12) results in the following real and imaginary equations which must be satisfied identically for the determinant of equation (8) to be zero:

$$\left.\begin{aligned}
\text{Re:}\quad & Q\left(\frac{\lambda}{\pi^4}\right)^4 + \left\{R_o - 2\left(\frac{8}{3}\right)^2 \bar{B}_I^{\,2}\left[\cos^2\Lambda + \left(\frac{a}{b}\right)^2 \sin^2\Lambda\right]\right\}\left(\frac{\lambda}{\pi^4}\right)^2 + S_o + \bar{B}_I^{\,4} - k\bar{B}_I^{\,2} = 0 \\
\text{Im:}\quad & \left(\frac{\lambda}{\pi^4}\right)^2 = \frac{e\bar{B}_I^{\,2} - p}{d}
\end{aligned}\right\} \tag{19a}$$

where

$$\left.\begin{aligned}
R_o &= \left(\bar{b}_1\bar{b}_2 + \bar{b}_3\bar{b}_4\right)\left(\frac{8}{3}\cos\Lambda\right)^2 + \left(\bar{b}_1\bar{b}_3 + \bar{b}_2\bar{b}_4\right)\left(\frac{8}{3}\frac{a}{b}\sin\Lambda\right)^2 \\
S_o &= \bar{b}_1\bar{b}_2\bar{b}_3\bar{b}_4 \\
p &= \left(\bar{b}_1 + \bar{b}_2\right)\bar{b}_3\bar{b}_4 + \bar{b}_1\bar{b}_2\left(\bar{b}_3 + \bar{b}_4\right) \\
d &= \left(\frac{8}{3}\right)^2\left(\bar{b}_1 + \bar{b}_2 + \bar{b}_3 + \bar{b}_4\right)\left[\cos^2\Lambda + \left(\frac{a}{b}\right)^2\sin^2\Lambda\right] \\
k &= \bar{b}_1\left(\bar{b}_2 + \bar{b}_3 + \bar{b}_4\right) + \bar{b}_2\left(\bar{b}_3 + \bar{b}_4\right) + \bar{b}_3\bar{b}_4 \\
e &= \bar{b}_1 + \bar{b}_2 + \bar{b}_3 + \bar{b}_4
\end{aligned}\right\} \tag{19b}$$

and

$$\left.\begin{aligned}
\bar{b}_1 &= 1 - \bar{A} - \bar{B}_R \\
\bar{b}_2 &= 16 - 4\bar{A} - \bar{B}_R \\
\bar{b}_3 &= 1 - \bar{A} - \bar{B}_R + 6\left(\frac{a}{b}\right)^2 \frac{D_{xy}}{D_x} - 3\left(\frac{a}{b}\right)^2\left[K_y \frac{N_y}{N_{y,cr}} - 5\left(\frac{a}{b}\right)^2 \frac{D_y}{D_x}\right] \\
\bar{b}_4 &= 16 - 4\bar{A} - \bar{B}_R + 24\left(\frac{a}{b}\right)^2 \frac{D_{xy}}{D_x} - 3\left(\frac{a}{b}\right)^2\left[K_y \frac{N_y}{N_{y,cr}} - 5\left(\frac{a}{b}\right)^2 \frac{D_y}{D_x}\right]
\end{aligned}\right\} \tag{19c}$$

The dynamic-pressure parameter λ can be eliminated between the real and imaginary parts of equations (19a). This will result in an equation in $\bar{A}$, $\bar{B}_R$, and $\bar{B}_I$ or an equation in $\bar{A}$ and $\left(\frac{\omega}{\omega_r}\right)^2$. Then for a specified stress condition and for specified values of g_a, the value of $\bar{B}_R$ or $\left(\frac{\omega}{\omega_r}\right)^2$ for flutter is obtained; the last of equations (19a) is then used to determine the critical value of λ.

Representative values of g_a were used in calculations presented in reference 6 for stressed, semi-infinite isotropic panels and in reference 8 for square, simply supported isotropic panels; these results showed negligible effect on the flutter boundaries. It is assumed that similar effects are obtained for simply supported orthotropic panels also. It should be noted, however, that aerodynamic damping may not be negligible for clamped panels and for long narrow panels. In this investigation numerical results will be obtained from equations (19a) only for the case in which g_a approaches zero. Equation (17) shows that when g_a is vanishingly small flutter occurs for $\bar{B}_I \approx 0$. Thus, equations (19a) reduce to

$$\text{Re:} \quad Q\left(\frac{\lambda}{\pi^4}\right)^4 + R_o\left(\frac{\lambda}{\pi^4}\right)^2 + S_o = 0 \tag{20}$$

and

$$\text{Im:} \quad \left(\frac{\lambda}{\pi^4}\right)^2 = -\frac{p}{d} \tag{21}$$

It should be remembered that neglect of g_a is the same as omitting the first-order time-derivative term of equation (1). Then, the linearized air forces in equation (1) reduce to the Ackeret value and (see, for example, ref. 7) a variety of combinations of λ, $\bar{A}$, and $\bar{B}_R$ correspond to simple harmonic motion. These conditions are given by solution of equation (20) alone. However, simultaneous solution of equations (20) and (21) specifies only those values of λ, $\bar{A}$, and $\bar{B}_R$ for which the circular frequency ω of harmonic vibration is on the verge of becoming complex; hence, the panel is on the verge of becoming dynamically unstable. Eliminating λ from these equations gives the following equation in terms of $\bar{B}_R$ and $\bar{A}$ only:

$$Qp^2 - R_o pd + S_o d^2 = 0 \tag{22}$$

Thus, for a given value of $\bar{A}$ and flow angle Λ, equation (22) is solved directly for the value of $\bar{B}_R$ for which flutter will occur. Then, substituting this value of $\bar{B}_R$ into equation (21) gives the value of λ for flutter.

Reduction of Equations at Flow Angles of 0° and 90°

At the extreme flow angles of 0° and 90° the solution to equation (22) can be simplified further. Substitution of equations (18) into equation (22) results, after considerably rearranging, in the following:

$$\cos^4\Lambda\left(\bar{b}_1 + \bar{b}_2\right)\left(\bar{b}_3 + \bar{b}_4\right)\left(\bar{b}_1\bar{b}_2 - \bar{b}_3\bar{b}_4\right)^2 + \left(\frac{a}{b}\right)^4\sin^4\Lambda\left(\bar{b}_1 + \bar{b}_3\right)\left(\bar{b}_2 + \bar{b}_4\right)\left(\bar{b}_1\bar{b}_3 - \bar{b}_2\bar{b}_4\right)^2$$

$$+ 2\left(\frac{a}{b}\right)^2\cos^2\Lambda\,\sin^2\Lambda\left\{\frac{1}{2}\left(\bar{b}_1 + \bar{b}_2 + \bar{b}_3 + \bar{b}_4\right)\left[\bar{b}_1\bar{b}_4\left(\bar{b}_2^{\,2} + \bar{b}_3^{\,2}\right)\left(\bar{b}_1 + \bar{b}_4\right)\right.\right.$$

$$\left.\left. + \bar{b}_2\bar{b}_3\left(\bar{b}_1^{\,2} + \bar{b}_4^{\,2}\right)\left(\bar{b}_2 + \bar{b}_3\right)\right] + \left[\left(\bar{b}_1 + \bar{b}_2\right)\bar{b}_3\bar{b}_4 + \bar{b}_1\bar{b}_2\left(\bar{b}_3 + \bar{b}_4\right)\right]^2\right\} = 0 \tag{23}$$

Thus, for flow angles of 0° or 90°, only the parenthetical quantities of the first and second terms, respectively, are retained. It is immediately apparent that in either case the equation has two distinct roots and one double-valued root. By definition, each root represents the conditions on the threshold of instability. However, for the double-valued root the physical significance is not obvious but will be discussed in a later section. For flow angles of 0° or 90°, equating the appropriate parenthetical terms of equation (23) to zero and substituting into equation (21) for p and d greatly reduce the labor of calculating the corresponding flutter values of λ. For $\Lambda = 0^\circ$ the following equations result:

$$\left.\begin{aligned} \bar{b}_1 + \bar{b}_2 &= 0 \\ \frac{\lambda_1}{\pi^4} &= \frac{3}{8}\left|\bar{b}_1\right| \end{aligned}\right\} \tag{24}$$

$$\left.\begin{aligned} \bar{b}_3 + \bar{b}_4 &= 0 \\ \frac{\lambda_2}{\pi^4} &= \frac{3}{8}\left|\bar{b}_3\right| \end{aligned}\right\} \tag{25}$$

and

$$\left.\begin{aligned} \bar{b}_1\bar{b}_2 - \bar{b}_3\bar{b}_4 &= 0 \\ \frac{\lambda_3}{\pi^4} &= \frac{3}{8}\sqrt{-\bar{b}_1\bar{b}_2} \end{aligned}\right\} \tag{26}$$

Thus, for a given value of $\bar{A}$, all flutter values of $\bar{B}_R$ are obtained from the first of equations (24) to (26); and the lowest corresponding flutter value of λ obtained from the last of equations (24) to (26) is termed λ_{cr}.

Equations similar to equations (24) to (26) are obtained for a flow angle of 90°. When the same procedure as before is followed, the parenthetical quantities of the second term from equation (23) result in the following equations for evaluating $\bar{B}_R$ and λ corresponding to flutter:

$$\left.\begin{aligned} \bar{b}_1 + \bar{b}_3 &= 0 \\ \frac{\lambda_1}{\pi^4} &= \frac{3}{8}\left|\bar{b}_1\right| \end{aligned}\right\} \tag{27}$$

$$\left.\begin{aligned} \bar{b}_2 + \bar{b}_4 &= 0 \\ \frac{\lambda_2}{\pi^4} &= \frac{3}{8}\left|\bar{b}_2\right| \end{aligned}\right\} \tag{28}$$

and

$$\left.\begin{aligned} \bar{b}_1\bar{b}_3 - \bar{b}_2\bar{b}_4 &= 0 \\ \frac{\lambda_3}{\pi^4} &= \frac{3}{8}\sqrt{-\bar{b}_1\bar{b}_3} \end{aligned}\right\} \tag{29}$$

It is worth noting here the modes that enter into the equations for λ. For $\Lambda = 0^\circ$, equations (24) show that the parameters $\bar{b}_1$ and $\bar{b}_2$ are sufficient to determine λ_1; these parameters are seen to be functions of modes associated with the coefficients C_{11} and C_{21} only (see eq. (8)) and, thus, modes with $n = 1$ are independent of modes with $n = 2$. The equation for λ_1 (eqs. (24)) reduces to equation (16) of reference 7 for isotropic panels where the modes associated with the coefficients C_{11} and C_{21} were used. Likewise, from equations (25) λ_2 is seen to be a function only of the modes associated with the coefficients C_{12} and C_{22}; however, equations (26) are related by all four modes. Parallel conditions exist for $\Lambda = 90^\circ$, as seen from equations (27) to (29).

Critical Buckling Loads

The foregoing equations for flutter of stressed panels are valid only to the point of buckling; hence, it will be useful to consider the buckling characteristics of orthotropic panels. The buckling characteristics are functions of the

length-width ratio a/b and the stiffness ratios D_y/D_x and D_{xy}/D_x. The range of stiffness ratios for this investigation will be limited to those appropriate to corrugation-stiffened panels (corrugated sheet with a single cover sheet). The lower limits of this range have been taken from reference 9 in which several different geometrical shapes of corrugations were considered. The minimum values found for the stiffness ratios were $\frac{D_{xy}}{D_x} = 0.15$ and $\frac{D_y}{D_x} = 0.0002$. Arbitrary upper limits on the stiffness ratios which will be used in subsequent calculations are $\frac{D_{xy}}{D_x} = 0.50$ and $\frac{D_y}{D_x} = 0.02$.

The equation for the critical buckling loads at zero airspeed, in terms of length-width ratio and stiffness ratios, is obtained directly from equation (5) by setting $\lambda = \alpha = 0$ and is

$$\left(\frac{mb}{a}\right)^2 N_{x,cr} + n^2 N_{y,cr} = \frac{\pi^2 D_x}{a^2}\left[m^4\left(\frac{b}{a}\right)^2 + n^4\left(\frac{a}{b}\right)^2 \frac{D_y}{D_x} + 2m^2n^2 \frac{D_{xy}}{D_x}\right] \tag{30}$$

Buckling coefficients for several buckling modes are plotted in figure 2 for a square panel ($a = b$) with stiffness ratios $\frac{D_{xy}}{D_x} = 0.15$ and $\frac{D_y}{D_x} = 0.0002$. In the figure the coordinates are the dimensionless coefficients K_x and K_y which are related to the critical inplane loads $N_{x,cr}$ and $N_{y,cr}$ by equations (11). The lines represent the variation of the buckling coefficients for various stress ratios N_y/N_x and the numbers on the lines denote the buckling modes which correspond to the m and n terms in the series expansion (eq. (4)). Calculations were made to include the first buckling mode for all compressive stress conditions; but, for clarity, some of the higher intermediate modes have been omitted. For $N_x = 0$ ($K_x = 0$), the lowest buckling mode corresponds to the coefficient C_{18}; as K_x is increased, several values of K_y/K_x or N_y/N_x result in equal choices of buckling modes. At a stress ratio $\frac{N_y}{N_x} = 0.3$ the buckling mode can be associated with either C_{11} or C_{12}; for stress ratios less than this value, the buckling mode corresponds to C_{11}. It is interesting to note that for $K_y = 0$ $(N_y = 0)$, $K_x = 1.3$ at the point of buckling; thus, for the specified panel conditions, the orthotropic panel has only slightly better load-carrying capability than a pinned-end column with the equivalent stiffness D_x. The insert in figure 2 shows the variation of the buckling coefficients with K_y extended into the region of tension and will be referred to in later discussion.

RESULTS AND DISCUSSION

As is seen from equations (20) and (21), flutter solutions are dependent on four basic parameters: the dynamic-pressure parameter λ, the stress parameter $\bar{A}$, the frequency parameter $\bar{B}_R$, and the flow angle Λ. For the unstressed panel, these parameters are, in turn, dependent on the length-width ratio a/b and the panel stiffness ratios; for flutter of a stressed panel, the stress ratio N_y/N_x and the critical stress parameter $K_x \frac{N_x}{N_{x,cr}}$ must also be specified. To explore in detail the effects of each of the variables on panel flutter would indeed be a lengthy process and, in fact, unwarranted in a four-mode analysis. It will be useful, however, to illustrate some of the more important effects of the various parameters on flutter characteristics of orthotropic panels. Thus, in the subsequent sections numerical results are presented only for a square panel ($a = b$) for several conditions of flow angularity, stiffness ratios, and inplane loads.

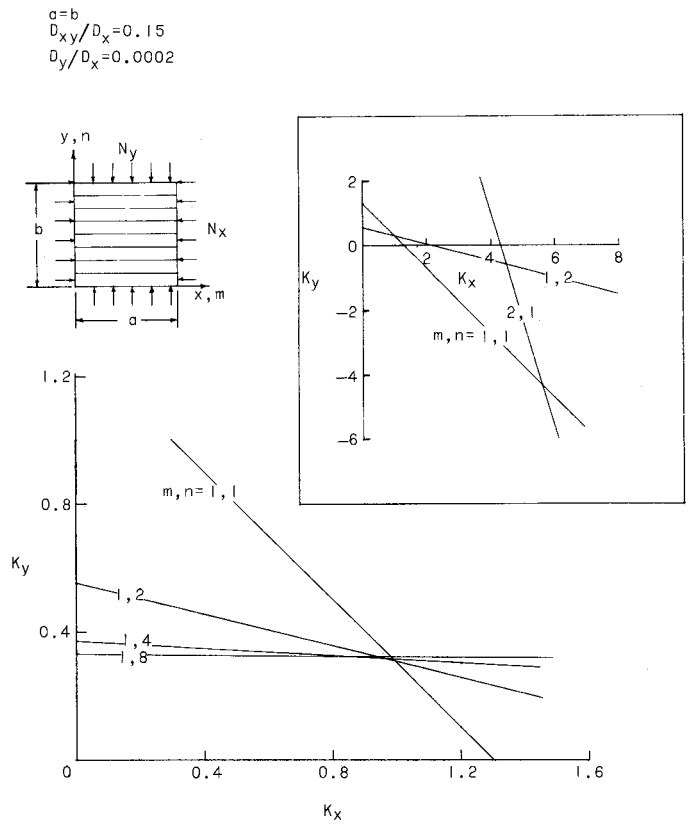

Figure 2.- Critical combinations of direct biaxial-load coefficients for flat simply supported orthotropic panel for selected m,n and with no airflow. $N_{x,cr} = K_x \frac{\pi^2 D_x}{a^2}$; $N_{y,cr} = K_y \frac{\pi^2 D_x}{a^2}$.

Effects of Flow Angularity on Flutter

The effects of flow angularity on flutter of orthotropic panels are shown in figure 3 where values of the dynamic-pressure parameter λ are plotted against the frequency parameter $\bar{B}_R$ for values of the flow angle Λ of 0°, 2°, and 90°. The calculations were made for $N_x = N_y = 0$, $a = b$, $\frac{D_{xy}}{D_x} = 0.15$, and $\frac{D_y}{D_x} = 0.0002$. The results shown in figure 3 were obtained from solutions of the real and imaginary parts of the flutter determinant (eqs. (20) and (21)). The loops shown by the solid curves are solutions of equation (20) and represent the variation of the panel frequencies with airflow. Note that for $\lambda = 0$ the four values of $\bar{B}_R$ correspond to the four natural frequencies in a vacuum (for vanishingly small values of damping) for the assumed modes; these modes are indicated by the C_{mn} terms at the base of the loops in figure 3. The dashed

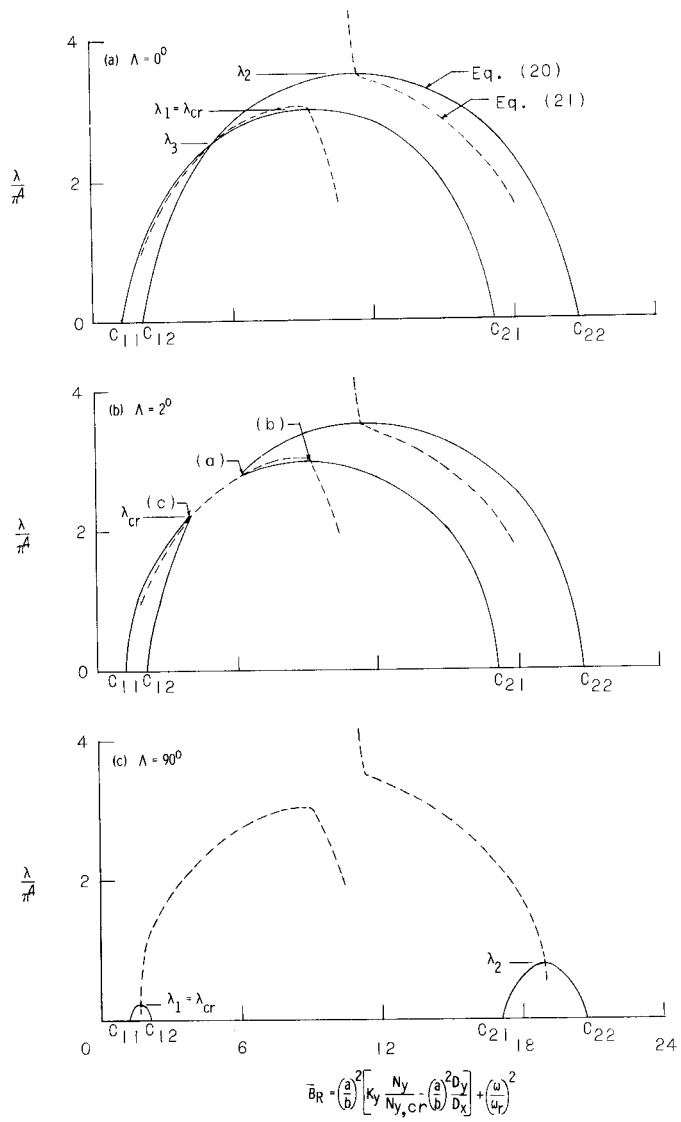

Figure 3.- Influence of airflow on panel frequency parameter $\bar{B}_R$ for flow angles of 0°, 2°, and 90°; associated C_{mn} are indicated for $\lambda = 0$. $a = b$; $N_x = N_y = 0$; $\frac{D_y}{D_x} = 0.0002$; $\frac{D_{xy}}{D_x} = 0.15$.

curves correspond to solutions of equation (21) and, thus, the intersections of the dashed curves with the solid curves specify the values of λ and $\bar{B}_R$ for which the real and imaginary parts of the flutter determinant are identically satisfied. The values of $\bar{A}$ and $\bar{B}_R$ at these intersection points are obtained directly from equation (22). It is interesting to note that minimization of λ with respect to the frequency parameter $\bar{B}_R$ from equation (20) leads directly to equation (21). Therefore, solutions to equations (20) and (21) always intersect wherever the frequency loops (solid curves) in figure 3 have zero slope. Thus, the contention of Hedgepeth (ref. 7) that flutter is imminent at coalescence of panel frequencies (under the assumption of zero aerodynamic damping) is further substantiated.

At the extreme flow angles of 0° and 90° (figs. 3(a) and 3(c), respectively) the intersections of the solid curves and dashed curves, denoted by λ_1, λ_2, and λ_3, are readily obtained from equations (24) to (26) for $\Lambda = 0°$ and from equations (27) and (28) for $\Lambda = 90°$. The lowest such value of λ is the critical value for flutter (denoted λ_{cr}), provided that for values of $\lambda > \lambda_{cr}$ the corresponding values of $\bar{B}_R$ become complex (hence, a mode of instability). Note that in figure 3(a) ($\Lambda = 0°$) there is a value of $\lambda < \lambda_{cr}$ for which two values of $\bar{B}_R$ are equal. The flutter solution at this intersection is given by the double-valued roots noted previously (see eq. (23)), and the corresponding values of $\bar{B}_R$ and Λ are obtained from equations (26). On the basis of the present analysis, this point is not clearly shown to be a point of instability because, for larger values of λ, the corresponding roots ω of the frequency parameter $\bar{B}_R$ remain real. Additionally,

in reference 4 it is reasoned that the modes at this intersection which are associated with the coefficients C_{11} and C_{12} will not couple aerodynamically at precisely zero flow angle. However, the solution at this point is degenerate and a linear instability of the form $te^{\alpha t}$ is entirely possible. In any event, the system is shown to verge on instability; however, the appropriate variable is not λ but the flow angle Λ itself, as will be shown presently. At a flow angle of 2° (fig. 3(b)) the frequency loops have separated and an actual coupling of the C_{11} and C_{12} modes is apparent. Furthermore, there are four intersections of the real and imaginary parts of the determinant, and, thus, four boundary points between stability and instability. The lowest critical value of λ occurs at the point labeled (c) and the system is unstable until λ is increased to a value corresponding to point (a). Now, however, there are again four roots of $\bar{B}_R$, all real, and all modes of oscillation are stable. Thus we have the odd result of a stable region between the values of λ at points (a) and (b), above and below which the panel is unstable. For increases in λ above the point (b) there will always be at least one mode of instability.

The flutter boundary for all flow angles between 0° and 90° (for zero stress) is shown in figure 4. In the regions below the boundary in figure 4 all four

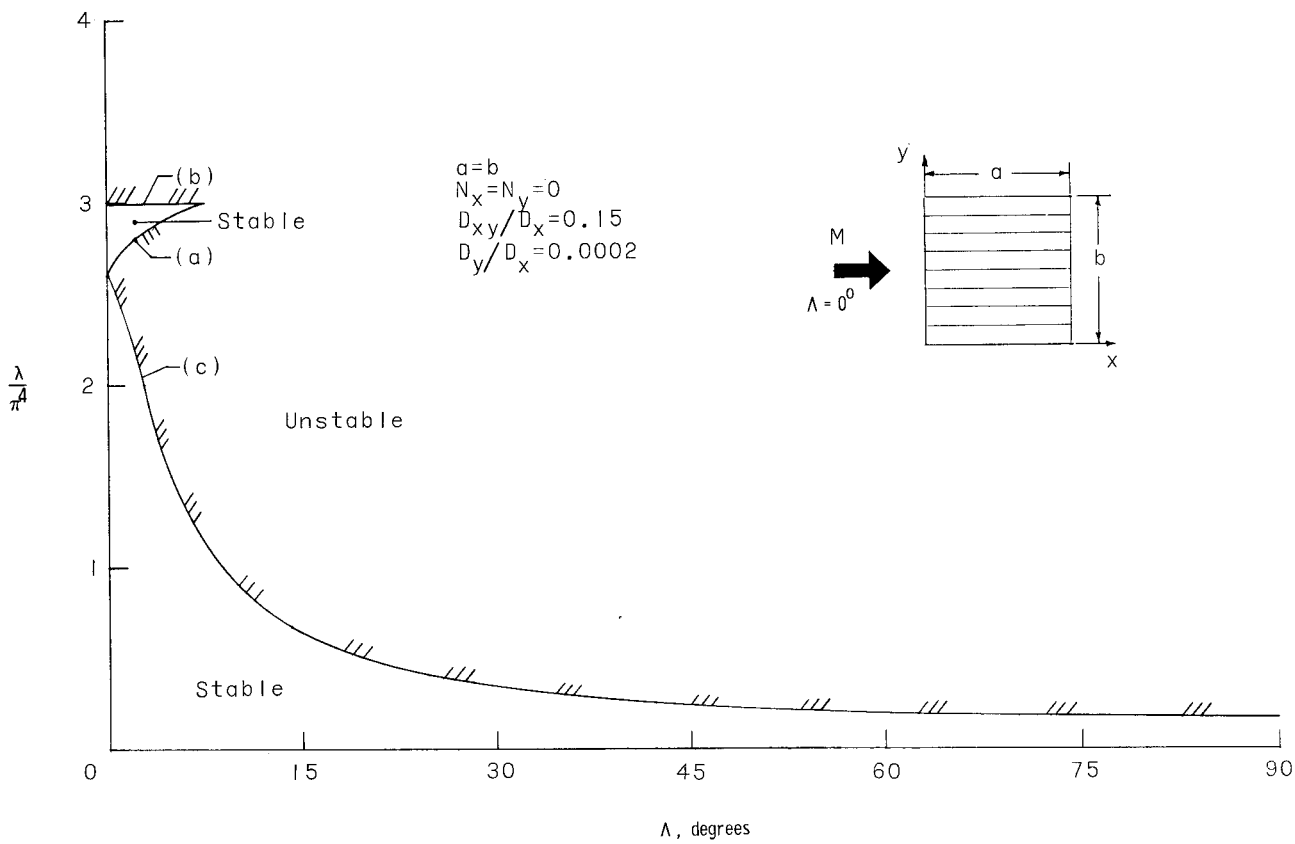

Figure 4.- Stability boundaries of orthotropic panel for arbitrary flow direction.

roots of the frequency parameter $\overline{B}_R$ are real and, thus, the panel is stable; in the region designated as unstable, at least two roots of $\overline{B}_R$ are complex conjugates and an unstable mode of oscillation exists. The boundaries labeled (a), (b), and (c) in figure 4 correspond to the points (a), (b), and (c), respectively, in figure 3(b). The stable region between boundaries (a) and (b) is shown to shrink rapidly with an increase in flow angle and disappears at approximately $\Lambda = 7^{\circ}$. At small angles Λ the boundaries (a) and (c) approach each other as the flow angle is decreased and they become coincident at exactly 0°. Hence, the frequency crossing (fig. 3(a)) given by the double-valued root of equation (23) has at least neutral stability (for $g_a = 0$) at a flow angle of 0°; however, the panel becomes unstable for any increase in flow angle, no matter how small. This bounded region of stability accounts for the apparent abrupt change in mode and the discontinuity in flutter boundaries shown in references 3 and 4 for isotropic panels of length-width ratios less than 1.0.

The practical significance of the stable region between boundaries (a) and (b) is somewhat difficult to assess. Such bounded regions of stability may exist for many orthotropic panels wherein the streamwise stiffness D_x is considerably greater than the cross-flow stiffness D_y. The size of the region appears to be dependent on the proximity of the frequency of the lowest antisymmetric mode (C_{12}) to the first natural frequency (C_{11}). Although the bounded stable region shown in figure 4 is small, the existence of such a region could result in scatter of experimental data of investigations where the flow angle is not considered. On the other hand, such a stable region appears to be of little consequence to the designer as this region dissipates rapidly with flow angle (at least for the orthotropic panel considered), and the lower curve (c) becomes the critical stability boundary.

The flutter boundary labeled (c) in figure 4 shows a pronounced effect of flow angle. For the stiffness ratios considered, the critical value of the dynamic-pressure parameter at $\Lambda = 90^{\circ}$ is only 6.8 percent of the value of boundary (c) at zero degrees. Thus, there appears to be a marked advantage of orienting the maximum panel flexural stiffness in the direction of the stream. However, the flow angle may be expected to vary in flight, with variations up to 30° not unreasonable for lifting reentry-type vehicles. Inasmuch as such an orientation away from an initial orientation of 0° would reduce λ_{cr} by 86 percent, the practical value of initial orientation of maximum stiffness in the stream direction is open to question.

The variation of λ_{cr} with flow angle for changes in the stiffness ratio D_{xy}/D_x is shown in figure 5. The curves were obtained for an unstressed panel with $\frac{D_{xy}}{D_x} = 0.15$, 0.30, and 0.50 and with $\frac{D_y}{D_x} = 0.0002$. Only the most critical boundaries corresponding to curve (c) from figure 4 are shown; the lower curve is reproduced from figure 4. As can be seen from figure 5, increases in stiffness ratio D_{xy}/D_x with constant D_y/D_x indicate a general increase in λ_{cr} over the entire range of flow angles.

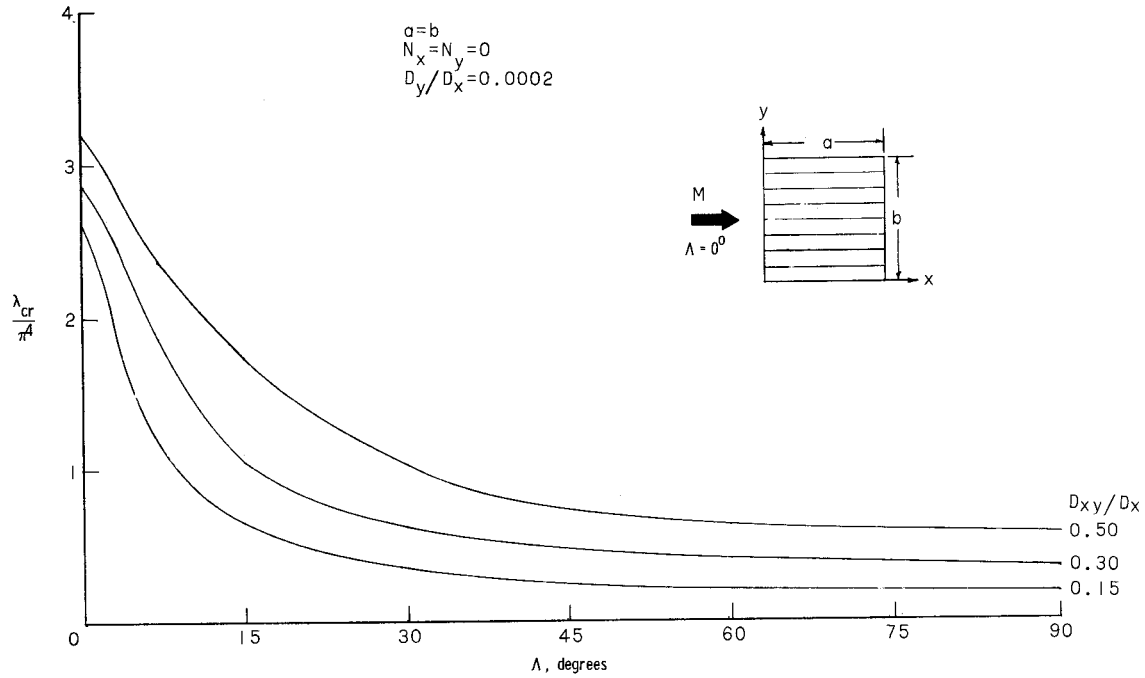

Figure 5.- Variation of critical dynamic-pressure parameter with flow angle for various stiffness ratios D_{xy}/D_x.

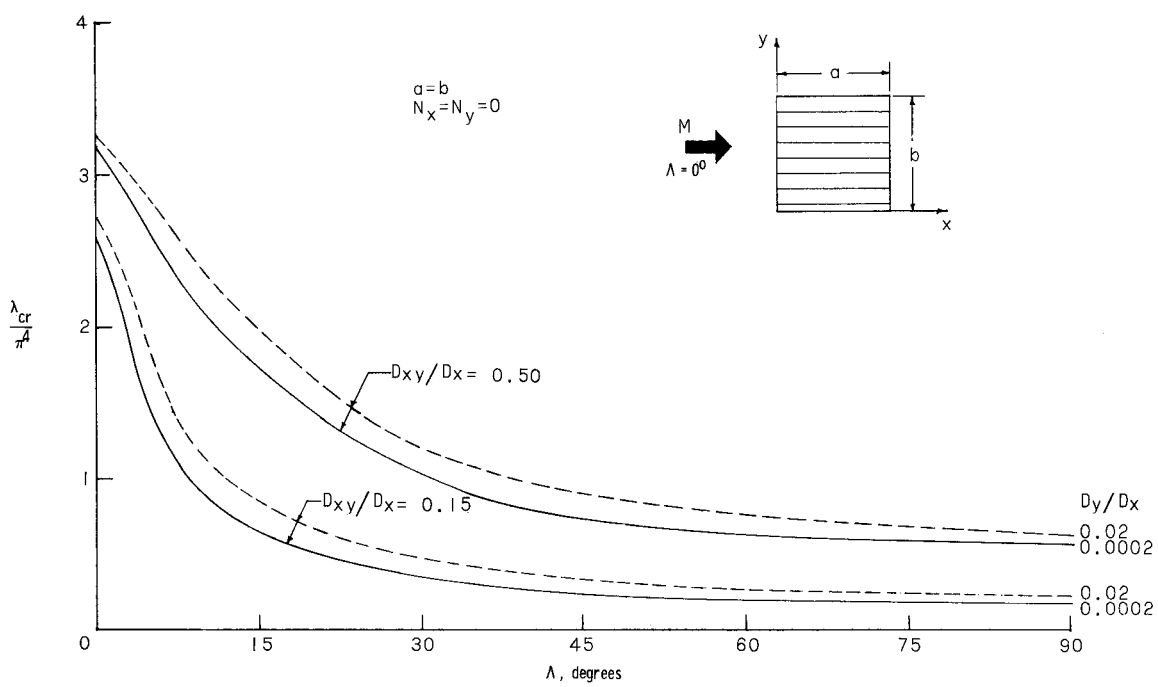

Figure 6.- Effects of stiffness ratio D_y/D_x on critical dynamic-pressure parameter.

The variation of λ_{cr} with flow angle for changes in the stiffness ratio D_y/D_x is shown in figure 6. The solid curves are reproduced from figure 5 and correspond to the stiffness ratios of $\frac{D_{xy}}{D_x} = 0.15$ and 0.50. The dashed curves represent the effects of an increase in the value of the stiffness ratio D_y/D_x from 0.0002 to 0.02. As can be seen from figure 6, only small increases in λ_{cr} are realized for the rather substantial increase in D_y/D_x. For example, for the curves corresponding to $\frac{D_{xy}}{D_x} = 0.15$ at $\Lambda = 90^\circ$, a stiffness ratio of $\frac{D_y}{D_x} = 0.02$ resulted in an increase in λ only 1.3 times the value for $\frac{D_y}{D_x} = 0.0002$. Thus, for the range of stiffness ratios considered, the flexural stiffness D_y is seen to have little effect on the flutter boundary.

Effects of Inplane Loads at Various Flow Angles

Recent experimental investigations (see refs. 10 to 14) and theoretical studies (refs. 4 and 15) on isotropic panels have revealed that panel susceptibility to flutter increases with application of compressive inplane loads and that generally the most susceptible condition occurs for the panel on the verge of buckling or at the transition from a flat-panel flutter boundary to a buckled-panel flutter boundary. Thus, calculations have been made to determine the effects of uniform inplane loads at arbitrary flow angles for the panel stiffness ratios of $\frac{D_y}{D_x} = 0.0002$ and $\frac{D_{xy}}{D_x} = 0.15$. Before various loading conditions are considered, however, it would be useful to examine the geometrical relationship of the basic flutter parameters contained in equation (20).

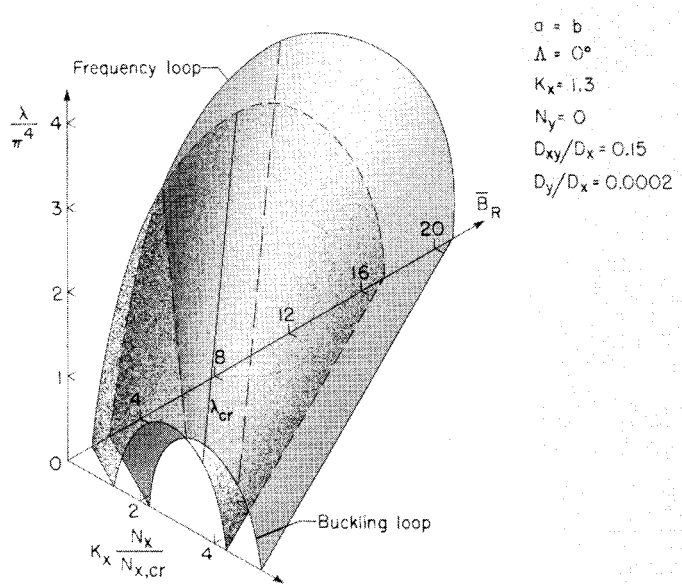

Figure 7.- Characteristic surfaces and associated flutter boundaries.

Vibration and buckling relations.- Solutions of equation (20) result in smooth surfaces which will be called "characteristic" surfaces. Such surfaces are shown in figure 7 on a plot of the flutter parameters: dynamic pressure λ, frequency $\bar{B}_R$, and stress $K_x \frac{N_x}{N_{x,cr}}$. The characteristic surfaces shown pertain to the panel oriented at zero flow angle and $N_y = 0$. A similar surface representing a two-mode solution is discussed in the appendix; however, some additional comments about the four-mode results are warranted here. The intersection of the surfaces in the zero λ-plane shows variations of

the panel in vacuo frequencies with stress. Planes of constant stress show the effects of airflow on the frequencies. Note that for zero stress, the characteristic surfaces trace the frequency variation as shown in figure 3(a). As pointed out in the discussion of figure 3, the roots of equation (22) locate the flutter points. Thus, for given stress conditions the solutions obtained result in the lines along the ridge of the characteristic surfaces and at the intersection of the two surfaces. Note from figure 7 that the character of the double-valued root observed at zero degrees is preserved for the stressed panel. For exactly zero flow angle, the flutter boundary corresponding to λ_{cr} is on the ridge (in planes of constant stress) of the lowest loop (see fig. 3(a)) and is shown in figure 7 as the solid line, whereas the intersection (dashed line) represents conditions on the verge of instability with variation of Λ.

The intercept of the characteristic surfaces with the zero frequency plane is shown by the loops in figure 7 for $\overline{B}_R = 0$ (for the panel conditions represented by fig. 7, $\overline{B}_R = -0.0002$ when $\omega = 0$). These loops indicate the effects of air forces on the static buckling loads. The flat-panel flutter boundary is valid to its intersection with a postbuckled flutter boundary; this intersection always lies above the intersection of the flat-panel flutter boundary and one of the buckling loops. (See ref. 15 and the appendix.) Thus, the latter intersection, which will govern the termination of the flat-panel flutter boundaries to be presented in later sections, may give a conservative estimate of the flutter speeds. Solution for the termination points is very simple and is illustrated in the appendix for a two-mode analysis. For the four-mode analysis presented herein, the termination points are obtained directly from equations (21) and (22) for arbitrary flow angle, when the frequency ratio ω/ω_r is set equal to zero in the expression for $\overline{B}_R$ (eqs. (18)); equation (22) is solved for $K_X \frac{N_X}{N_{X,cr}}$ which is substituted into equation (21) for λ_{cr}. Similarly, at the extreme flow angles ($\Lambda = 0^\circ$ and 90°) the reduced equations (eqs. (24) to (27)) permit rapid evaluation of the termination points.

The peaks of the buckling loops represent the conditions wherein loss of stable, static, buckled equilibrium occurs and, hence, is termed the "transtability" flutter speed. (See ref. 16 and the appendix.) As can be seen from figure 7, the termination points are somewhat removed from the peak of the loop.

The appearance of the characteristic surfaces for flow angles other than zero degrees may be visualized with the aid of figure 8, in which the buckling loops are shown for $\Lambda = 0^\circ$, 2°, and 90°, and with reference to the frequency loops shown in figure 3. The loops in figure 8 were obtained from equation (20) for $N_y = 0$ and $K_x = 1.3$. The intercepts of the critical flutter boundary with the loops, indicated by the circles, were obtained from equation (22) and/or the corresponding reduced equations for $\Lambda = 0^\circ$ and 90°. The dashed curves are portions of the corresponding critical flutter boundaries projected on the dynamic-pressure—stress plane.

Figure 8(a) corresponds to the buckling loops shown in figure 7 and indicates the difference in the transtability value and the termination point. In

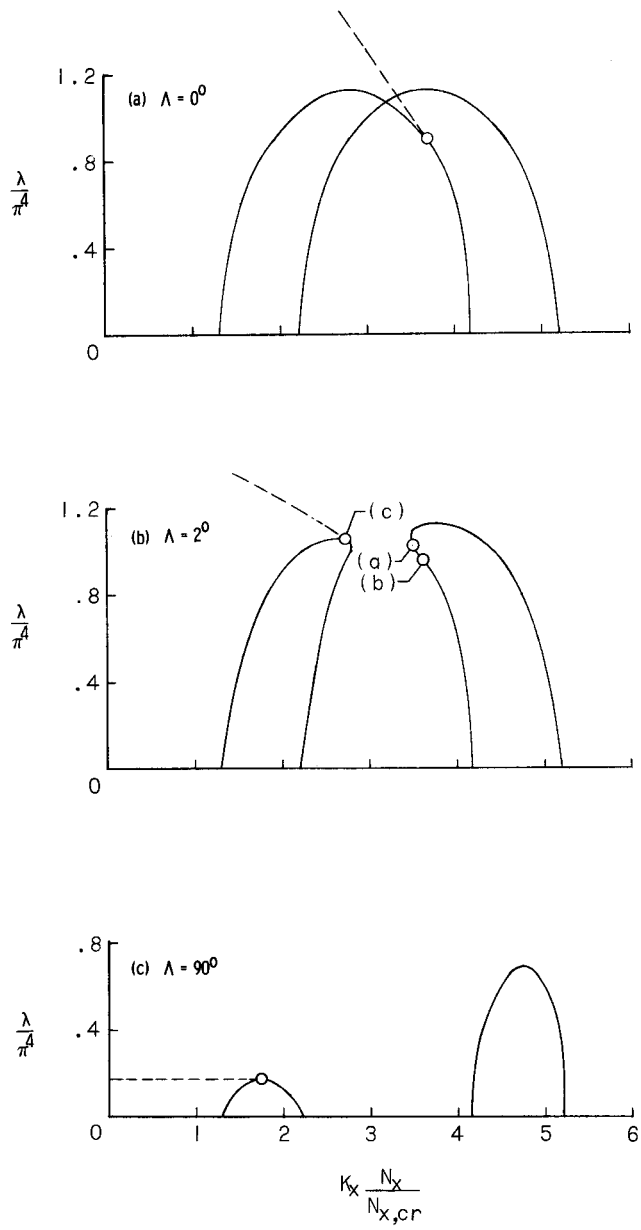

Figure 8.- Influence of airflow on buckling loads for flow angles of 0°, 2°, and 90°. $N_y = 0$; $K_x = 1.3$; $\frac{D_y}{D_x} = 0.0002$; $\frac{D_{xy}}{D_x} = 0.15$. (Dashed lines represent portion of flutter boundary.)

figure 8(b), for $\Lambda = 2^\circ$, the characteristic surfaces have separated as was the case shown in figure 3(b), and the flutter boundary now corresponds to that initially represented by the frequency crossing. As noted previously, the separation of the frequency loops lowered the critical value of the dynamic-pressure parameter for flutter of the unstressed panel (see, for example, fig. 4); however, as can be seen in figures 8(a) and 8(b), at the termination point the frequency separation results initially in an increase in the value of the dynamic-pressure parameter. In figure 8(c), for $\Lambda = 90^\circ$, the buckling loops and, thus, the characteristic surfaces, have degenerated into two independent surfaces.

Stability regions of a flat panel with inplane load.- Before the effects of inplane loads on flutter boundaries for a panel at arbitrary flow angles are considered, it would be interesting to investigate the effects of inplane loads on the bounded stability region shown in figure 4. The stability regions resulting from application of an inplane load N_x for flow angles of 0° and 2° are shown in figure 9. The calculations were made for stiffness ratios of $\frac{D_{xy}}{D_x} = 0.15$ and $\frac{D_y}{D_x} = 0.0002$ and for $K_x = 1.3$. The solid curves correspond to solutions for a flow angle of 0°, whereas the dashed curves and the upper solid curve represent solutions for a flow angle of 2°. The upper solid curve labeled (b) represents the flutter boundary at precisely zero degrees; the lower solid curve represents the frequency crossing shown in figure 7. The curves labeled (a), (b), and (c) show the variation of the respective flutter points from figure 3(b) with application of inplane load. The termination points (denoted by the circles) correspond to the points shown in figure 8(b) for $\Lambda = 2^\circ$.

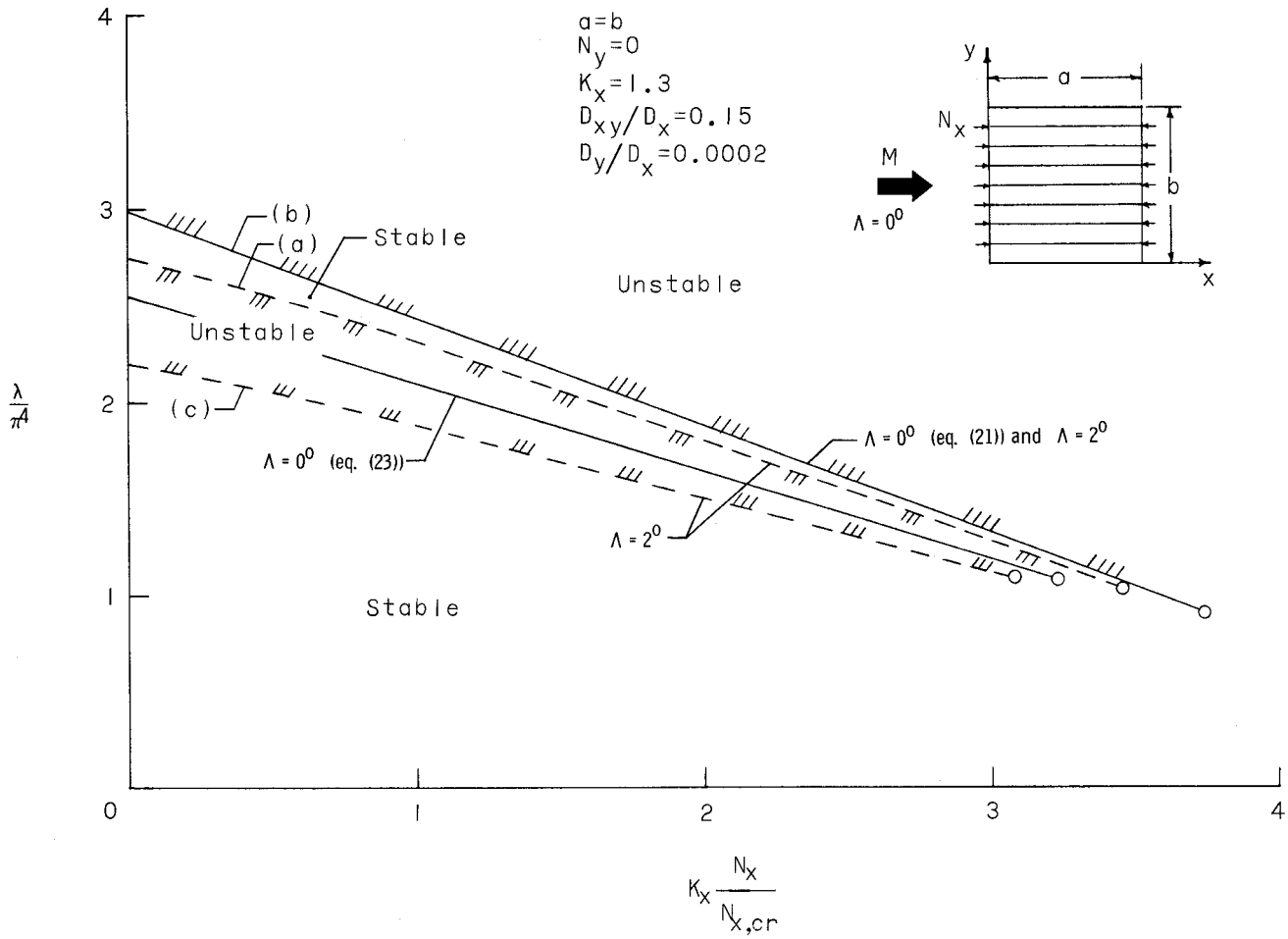

Figure 9.- Stability boundaries of flat panel with inplane compression for flow angles of 0° and 2°. Circles represent termination points.

As can be seen from figure 9, for $\Lambda = 2^o$ the small stable region exists over the entire flat-panel boundary. As the flow angle approaches 0°, the dashed curves (a) and (c) approach the lower solid curve and the unstable region disappears. As the flow angle is increased above 2°, the boundary (a) approaches the boundary (b) and, thus, the stable region disappears. Boundaries (a) and (b) were noted previously to coincide (for $N_x = 0$) at a flow angle of 7°.

The results shown in figure 9 could be of particular significance in experimental panel flutter investigations since the unstable region bounded by curves (a) and (c) could exist for only a slight deviation of flow angle from the true zero position. Thus, wind-tunnel investigations of a stressed panel could conceivably result in two distinct flat-panel flutter boundaries or, if not clearly delineated, could show up as apparent scatter in the data.

Effects of inplane load N_x at various flow angles.- Numerical solutions to equation (22) obtained for various values of $\frac{N_x}{N_{x,cr}}$ (to the termination point) and for flow angles of $\Lambda = 0^\circ$, 5°, 10°, 45°, and 90° are shown in figure 10. The calculations are based on $N_y = 0$ $(K_y = 0)$, for which $K_x = 1.3$ is obtained from figure 2. For $N_x = 0$, the values of the dynamic-pressure parameter at the different flow angles are those shown by the curve in figure 4. The boundary corresponding to $\Lambda = 0^\circ$ is reproduced from figure 9 for comparison with boundaries at other flow angles. The dashed line, representing the frequency crossing, is also shown since this boundary signifies the beginning of the unstable region as Λ is increased. At $\Lambda = 0^\circ$, λ_{cr} decreases linearly with increasing values of N_x. As the flow angle is increased, however, the flutter boundary is seen to be less dependent on the inplane load. At $\Lambda = 90^\circ$ the flutter boundary is independent of loading, inasmuch as the direction of inplane loading is at right

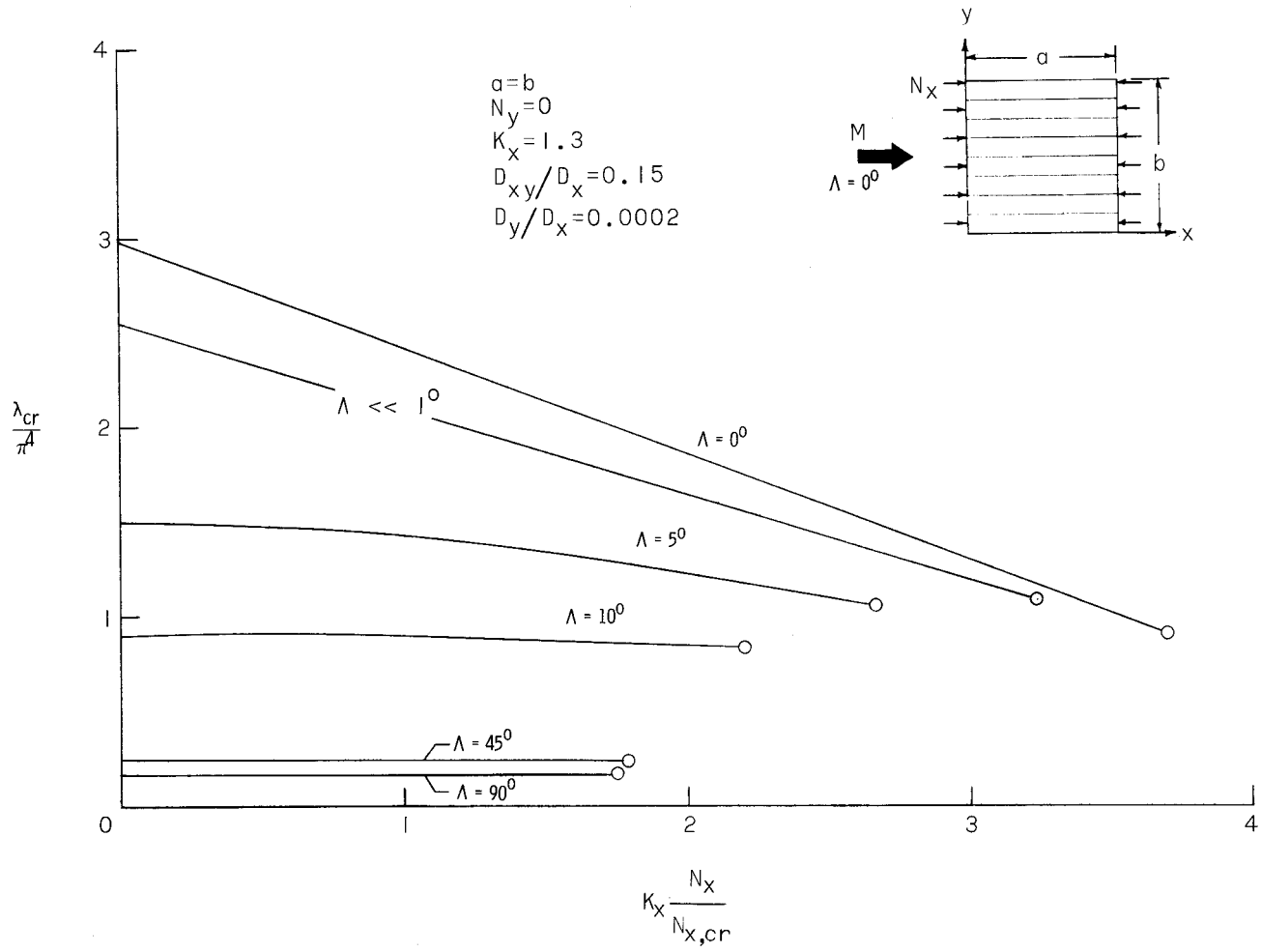

Figure 10.- Flutter boundaries as functions of inplane load N_x for various flow angles. Circles represent termination points.

angles to the direction of flow. A similar result was obtained in references 7 and 15. It should be noted that a small stable region exists above the curve for $\Lambda = 5^{\circ}$ (see fig. 4); however, this region is omitted here for simplicity.

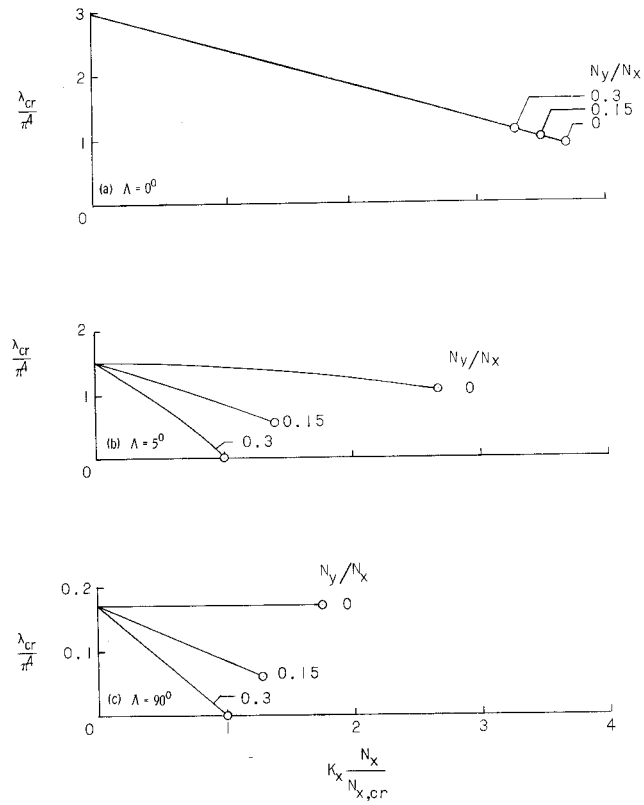

Figure 11.- Flutter boundaries as functions of stress ratio N_y/N_x for flow angles of 0°, 5°, and 90°. Circles represent termination points.

Effects of stress ratio N_y/N_x.- Flutter boundaries have been obtained for stress ratios of $\frac{N_y}{N_x} = 0.15$ and 0.3 at flow angles of $\Lambda = 0^{\circ}$, 5°, and 90°. For stress ratios greater than 0.3, higher mode buckling results (see fig. 2); thus, more modes would have to be used in the analysis. The flutter boundaries are shown in figure 11 where the dynamic-pressure parameter is plotted against the stress parameter $K_x \frac{N_x}{N_{x,cr}}$. Figure 11(a) shows the boundaries for $\Lambda = 0^{\circ}$, figure 11(b) for $\Lambda = 5^{\circ}$, and figure 11(c) for $\Lambda = 90^{\circ}$. The stress ratio for each curve is shown on the figure; the boundaries for $\frac{N_y}{N_x} = 0$ are reproduced from figure 10. In figure 11(a) a single boundary is obtained for all values of N_y/N_x, but the value of λ_{cr} at the termination point is different for each stress ratio. Thus, as was noted previously, the loading normal to airstream N_y does not change the position of the flutter boundary but simply determines the location of the termination point. The value of λ_{cr} at the termination point for a stress ratio of zero is only 30 percent of the value for no stress and represents a large increase in panel thickness for prevention of flutter. The addition of N_y raises the termination point and, thus at $\Lambda = 0^{\circ}$, appears to be beneficial. (It should be noted that an increase in N_y/N_x is not necessarily beneficial; see, for example, ref. 17.) However, the opposite is true for any other flow angle, as is shown by figures 11(b) and 11(c). Increases in the stress ratio result in decreases in the value of λ_{cr} for flutter until, at a stress ratio of 0.3, the value of λ_{cr} at the point of buckling goes to zero. The fact that λ_{cr} becomes zero is a result of the change in critical flutter modes (see fig. 3) associated with the separation of the characteristic surfaces. See, for example, the buckling chart shown in figure 2; at a stress ratio of 0.3 the panel has an equal choice of buckling modes (C_{11} and C_{12}), and, because these modes coalesce for flutter (for flow angles other than zero degrees), any increase in

λ results in flutter. The condition of zero λ, or infinite thickness, would probably be circumvented if nonlinear effects were considered. The phenomenon of infinite thickness for prevention of flutter is discussed in detail in reference 17. As noted previously, the change in critical flutter mode occurs instantaneously with a change in flow angle from the zero position; thus, the condition of infinite thickness exists over practically the entire range of flow angles.

Several conditions of midplane compression have been considered, but no mention has been made of effects of midplane tension. In general, tension is considered beneficial in the alleviation of panel flutter. However, this may not always be true if panel buckling is possible. Consider, for example, the case in which N_y is negative (tension) and N_x is in compression with the panel oriented at zero flow angle. Note from the insert on the buckling chart (fig. 2) that for a stress ratio of $\frac{N_y}{N_x} = -0.77$ the panel again has an equal choice of buckling modes $\left(C_{11} \text{ and } C_{21}\right)$. Note also from figure 3(a) that these two modes are critical for flutter at precisely $\Lambda = 0^{\circ}$; therefore, it can be concluded that again λ_{cr} becomes zero for flutter. Calculations show that the flutter boundary for negative N_y is actually an extension of the boundary in figure 11(a) where λ_{cr} continues to decrease linearly for negative increases of the stress ratio N_y/N_x.

CONCLUDING REMARKS

A theoretical analysis for flutter of flat rectangular simply supported orthotropic panels is presented. The lateral loading is obtained from modified piston theory aerodynamics. Numerical results (obtained for zero aerodynamic damping) are presented for arbitrary panel orientation with the airstream and for various conditions of biaxial compressive stress. The panel is oriented such that a flow angle of zero degrees corresponds to the direction of maximum panel flexural stiffness alined with the stream. All calculations are based on a panel length-width ratio of 1.0.

The results for an unstressed panel show that for prescribed stiffness ratios, representative of corrugation-stiffened panels, the panel oriented with the maximum flexural stiffness in the direction of the stream provides greatest resistance to flutter. However, flutter characteristics of orthotropic panels are found to be highly sensitive to variations in flow angularity from this orientation. Thus, the practical value of orientation of maximum stiffness in the direction of the stream is open to question. In the range of stiffness ratios considered, changes in the stiffness ratio D_{xy}/D_x were found to be effective in changing the flutter boundary; however, a large range of the stiffness ratio D_y/D_x was found to be rather ineffective on the flutter results.

Any deviation of the panel from the position of precisely zero flow angle was found to cause a change in the critical flutter mode. For small values of the flow angle, this mode change resulted in a region of stable oscillations

bounded completely by an unstable region; thus, the odd result that an increase in the airspeed may render an unstable panel stable. The bounded stable region was preserved with the inclusion of compressive inplane loads and resulted in two distinct flat-panel boundaries (in a small range of the flow angle from the zero position). Such characteristics could cause considerable discrepancy in experimental data if not taken into account. In addition, as a consequence of the change in critical flutter mode, for certain stress ratios, panels which require a finite thickness at buckling when oriented at zero flow angle require infinite thickness for all other flow angles. Thus, it is apparent that certain stress ratios must be avoided in design.

Langley Research Center,
National Aeronautics and Space Administration,
Langley Station, Hampton, Va., June 6, 1963.

APPENDIX

A METHOD FOR DETERMINING THE INTERSECTION OF DYNAMIC AND STATIC STABILITY BOUNDARIES

Experimental and theoretical investigations (see refs. 10 and 15) have shown that the most critical condition for flutter of a panel subjected to compressive inplane loads occurs at transition from the unbuckled to postbuckled flutter boundaries. A method for estimating the critical flutter speed at transition (in absence of a large-deflection analysis) is based on the transtability analysis introduced in reference 16; this analysis considers only the static buckling behavior of a panel (or beam) in the presence of supersonic flow. This approach has been shown to give a good approximation to the flutter speed for infinitely wide buckled panels (see ref. 18) and has been applied to three-dimensional isotropic panels in references 7 and 17.

The results of a recent large-deflection dynamic analysis of finite isotropic panels, presented in reference 15, indicate that the critical flutter speed at termination of the flat-panel flutter boundary may, in different cases, lie above or below the transtability speed and, thus, the transtability speed may be nonconservative. In no case, however, did the large-deflection flutter boundaries lie below that critical speed defined by the intersection of the flat-panel dynamic boundaries with the static stability boundaries. Hence, the critical speed at this intersection is used in this paper to terminate the flat-panel flutter boundaries. The method for obtaining the intersection of the dynamic boundary with the static stability boundary is presented in this appendix and the mathematical expressions are shown to be as simple as those for the transtability speed. The approach differs from the transtability concept in that the panel frequencies are retained in the equations and, thus, it permits a traceable relationship between the vibration, flutter, and buckling characteristics in the presence of supersonic airflow.

For purposes of simplicity, only a two-mode analysis will be made; that is, $j = 2$ and $l = 1$ (see eq. (5)). Further, simple harmonic motion is assumed, such that $\alpha = i\omega$, and damping is negligible ($g_a \approx 0$). Then for a zero flow angle ($\Lambda = 0^{\circ}$) the flutter determinant can be written, in the present notation, as shown:

$$\begin{vmatrix} \bar{b}_1 & \dfrac{8\lambda}{3\pi^4} \\ -\dfrac{8\lambda}{3\pi^4} & \bar{b}_2 \end{vmatrix} = 0 \tag{A1}$$

where

$$
\left.
\begin{aligned}
\bar{b}_1 &= 1 - \bar{A} - \bar{B}_R \\
b_2 &= 16 - 4\bar{A} - \bar{B}_R \\
\bar{A} &= K_x \frac{N_x}{N_{x,cr}} - 2\left(\frac{a}{b}\right)^2 \frac{D_{xy}}{D_x} \\
\bar{B}_R &= \left(\frac{a}{b}\right)^2\left[K_y \frac{N_y}{N_{y,cr}} - \left(\frac{a}{b}\right)^2 \frac{D_y}{D_x}\right] + \left(\frac{\omega}{\omega_r}\right)^2
\end{aligned}
\right\} \tag{A2}
$$

Note that the frequency parameter $\bar{B}_R$ contains the eigenvalue $\left(\frac{\omega}{\omega_r}\right)^2$. The solution to equation (A1) in terms of the frequency parameter $\bar{B}_R$, after some rearranging, is

$$
\bar{B}_R = \frac{17 - 5\bar{A}}{2} \pm \frac{3}{2}\sqrt{(\bar{A} - 5)^2 - \left(\frac{16\lambda}{9\pi^4}\right)^2} \tag{A3}
$$

Solutions to equation (A3) result in a characteristic surface like that shown in figure 12 on a plot of the three basic flutter parameters: dynamic pressure λ, frequency ratio $\left(\frac{\omega}{\omega_r}\right)^2$, and stress $\bar{A}$. Figure 12 is intended for illustrative purposes only; hence, the numerical values of λ and $\bar{A}$ are unimportant. However, the two-mode representation as shown is limited to panel configurations and stress conditions for which buckling occurs in the first mode. Additionally, it should be noted that the stress is not necessarily zero for $\bar{A} = 0$.

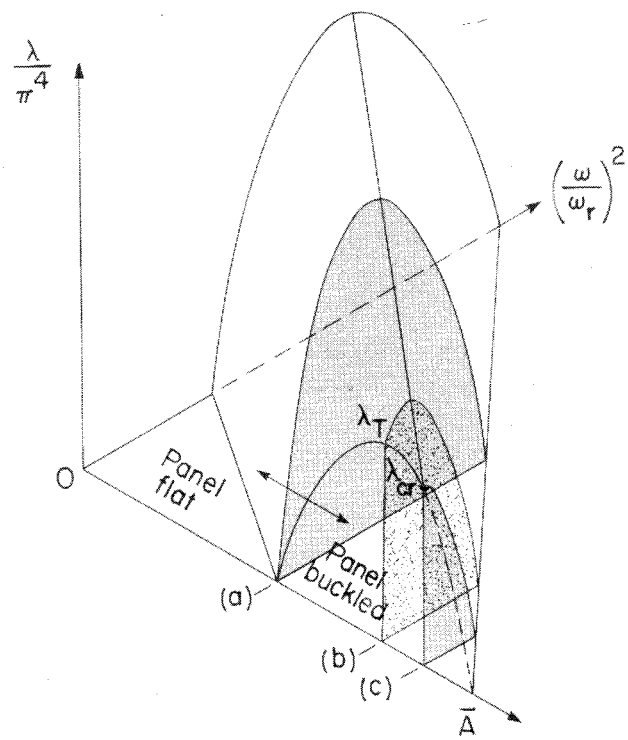

Figure 12.- Characteristic surface relating vibrations, buckling, and flutter. Trace in zero frequency plane shows variation of buckling load with airflow.

The intercept of the surface with the zero λ-plane shows the variation of panel frequencies with stress. The values of $\bar{A}$ at which the frequencies become zero correspond to the two static buckling loads for the assumed modes. Planes of constant stress show the variation of panel frequencies with airflow. Coalescence of the frequencies constitutes dynamic instability (for zero damping) and, hence, flutter (ref. 7), since the eigenvalues $\left(\frac{\omega}{\omega_r}\right)^2$ become

complex for values of λ above the peak of the frequency loop. Thus, the flat-panel dynamic boundary is represented by the solid ridge line of the characteristic surface. The intercept of the characteristic surface with the zero frequency plane, represented by the trace in the $\lambda\bar{A}$-plane, shows the variation of the panel buckling loads with airflow. This trace represents the static stability boundary and results when the frequency is set equal to zero in equation (A1); thus, the role of the eigenvalue is transferred to $\bar{A}$. Above the peak of the static boundary the loads disappear and, hence, from transtability considerations no stable, static buckled configuration exists. Thus, the peak of the static boundary (through which the plane labeled (b) in fig. (12) passes) constitutes the transtability speed λ_T. The intersection of the dynamic boundary with the static boundary (denoted λ_{cr}, and through which plane (c) passes) represents the value of λ for which the flutter frequency becomes zero, or, on the basis of small-deflection theory, λ_{cr} corresponds to buckling in the flutter mode. As seen from figure 12, λ_{cr} is less than λ_T.

The procedure for obtaining λ_{cr} is straightforward. Inasmuch as dynamic instability results when the frequencies coalesce or become equal, it is seen from equation (A3) that for flutter the radical term must always be zero. Hence,

$$\frac{\lambda}{\pi^4} = \frac{9}{16}\left|\bar{A} - 5\right| \tag{A4}$$

and thus equation (A3) becomes

$$\bar{B}_R = \frac{17 - 5\bar{A}}{2} \tag{A5}$$

Equations (A4) and (A5) are completely general and, thus, locate the flutter boundary for specified values of $\bar{A}$; equation (A4) is identical to that obtained in reference 7. Then the values of $\bar{A}$ and λ_{cr} at the intersection of the dynamic flutter boundary with the static stability boundary is obtained by setting the frequency ratio $\left(\frac{\omega}{\omega_r}\right)^2$ equal to zero in the expression for $\bar{B}_R$ (eqs. (A2)) and by substituting the result into equations (A4) and (A5).

It is of interest to note the relationship between λ_T and λ_{cr}; the difference in these values is dependent on the boundary conditions on inplane loads. Consider, for instance, the case in which the panel is loaded by N_x only $\left(N_y = 0\right)$. From equation (A2), $\bar{B}_R$ is a constant $\left(\text{for } \left(\frac{\omega}{\omega_r}\right)^2 = 0\right)$, and, hence, substituting $\bar{A}$ from equation (A5) into equation (A4) yields

$$\frac{\lambda_{cr}}{\pi^4} = \frac{9}{40}\left|\bar{B}_R + 4\right| \tag{A6}$$

and the corresponding value of λ_T, as shown in reference 7, is

$$\frac{\lambda_T}{\pi^4} = \frac{9}{32}\left|\bar{B}_R + 4\right| \tag{A7}$$

Thus, λ_T is 25 percent greater than λ_{cr}. On the other hand, if the loading is reversed $\left(N_x = 0\right)$, the flutter boundary is independent of the loading and, hence, $\lambda_T = \lambda_{cr}$ and is given by equation (A4).

The equations developed to obtain λ_{cr} (eqs. (A4) and (A5)) are readily converted to the form used in the text. Equation (A5) is seen to be the sum of the diagonal terms of equations (A2); that is,

$$\bar{b}_1 + \bar{b}_2 = 0 \tag{A8}$$

Further, upon substitution of $\bar{B}_R$ from equation (A5) into the equation for $\bar{b}_1$ from equations (A2), equation (A4) can be written as

$$\frac{\lambda_{cr}}{\pi^4} = \frac{3}{8}\left|\bar{b}_1\right| \tag{A9}$$

Equations (A8) and (A9) are seen to be identical to equations (24) of the text.

REFERENCES

1. Kordes, Eldon E., and Noll, Richard B.: Flight Flutter Results for Flat Rectangular Panels. NASA TN D-1058, 1962.

2. Fung, Y. C. B.: A Summary of the Theories and Experiments on Panel Flutter. AFOSR TN 60-224, Guggenheim Aero. Lab., C.I.T., May 1960.

3. Kordes, Eldon E., and Noll, Richard B.: Theoretical Flutter Analysis of Flat Rectangular Panels in Uniform Coplanar Flow With Arbitrary Direction. NASA TN D-1156, 1962.

4. Eisley, J. G., and Luessen, G.: The Flutter of Thin Plates Under Combined Shear and Normal Edge Forces Including the Effects of Varying Sweepback. Paper No. 62-90, Inst. Aerospace Sci., June 1962.

5. Kordes, Eldon E., Tuovila, Weimer J., and Guy, Lawrence D.: Flutter Research on Skin Panels. NASA TN D-451, 1960.

6. Houbolt, John C.: A Study of Several Aerothermoelastic Problems of Aircraft Structures in High-Speed Flight. Nr. 5, Mitteilungen aus dem Institut für Flugzeugstatik und Leichtbau. Leemann (Zürich), c.1958.

7. Hedgepeth, John M.: Flutter of Rectangular Simply Supported Panels at High Supersonic Speeds. Jour. Aero. Sci., vol. 24, no. 8, Aug. 1957, pp. 563-573, 586.

8. Movchan, A. A.: On the Stability of a Panel Moving in a Gas. NASA RE 11-21-58W, 1959.

9. Stroud, W. Jefferson: Elastic Constants for Bending and Twisting of Corrugation-Stiffened Panels. NASA TR R-166, 1963.

10. Dixon, Sidney C., Griffith, George E., and Bohon, Herman L.: Experimental Investigation at Mach Number 3.0 of the Effects of Thermal Stress and Buckling on the Flutter of Four-Bay Aluminum Alloy Panels With Length-Width Ratios of 10. NASA TN D-921, 1961.

11. Guy, Lawrence D., and Bohon, Herman L.: Flutter of Aerodynamically Heated Aluminum-Alloy and Stainless-Steel Panels With Length-Width Ratio of 10 at Mach Number of 3.0. NASA TN D-1353, 1962.

12. Bohon, Herman L.: Panel Flutter Tests on Full-Scale X-15 Lower Vertical Stabilizer at Mach Number 3.0. NASA TN D-1385, 1962.

13. Hess, Robert W., and Gibson, Frederick W.: Experimental Investigation of the Effects of Compressive Stress on the Flutter of a Curved Panel and a Flat Panel at Supersonic Mach Numbers. NASA TN D-1386, 1962.

14. Dixon, Sidney C.: Experimental Investigation at Mach Number 3.0 of Effects of Thermal Stress and Buckling on Flutter Characteristics of Flat Single-Bay Panels of Length-Width Ratio 0.96. NASA TN D-1485, 1962.

15. Fralich, Robert W.: Postbuckling Effects on the Flutter of Simply Supported Rectangular Panels at Supersonic Speeds. NASA TN D-1615, 1963.

16. Isaacs, R. P.: Transtability Flutter of Supersonic Aircraft Panels. U.S. Air Force Project RAND P-101, The RAND Corp., July 1, 1949.

17. Dixon, Sidney C.: Application of Transtability Concept to Flutter of Finite Panels and Experimental Results. NASA TN D-1948, 1963.

18. Fung, Y. C.: The Flutter of a Buckled Plate in Supersonic Flow. OSR-TN-55-237, Guggenheim Aero. Lab., C.I.T., July 1955.

NASA-Langley, 1963 L-3275